
Article:
Asenath-Smith, E, Noble, JM, Hovden, R et al. (7 more authors) (2017) Physical Confinement Promoting Formation of Cu2O−Au Heterostructures with Au Nanoparticles Entrapped within Crystalline Cu2O Nanorods. Chemistry of Materials, 29 (2). pp. 555-563. ISSN 0897-4756

https://doi.org/10.1021/acs.chemmater.6b03653

Title: Physical confinement promotes formation of Au/Cu_2O heterostructures with Au nanoparticles entrapped within crystalline Cu_2O nanorods

Authors: Emily Asenath-Smith,[a,*,1] Jade M. Noble,[2] Robert Hovden,[3] Amanda M. Uhl,[1] Allessandra DiCorato,[1] Yi-Yeoun Kim,[4] Alexander N. Kulak,[4] Fiona C. Meldrum,[4] Lena F. Kourkoutis[3,5] & Lara A. Estroff*[,1,5]

[1] Department of Materials Science and Engineering, Cornell University, Ithaca, New York 14853 (U.S.A.)

[2] Robert Frederick Smith School of Chemical and Biomolecular Engineering, Cornell University, Ithaca, New York,14853 (U.S.A.)

[3] School of Applied and Engineering Physics, Cornell University, Ithaca, New York 14853 (U.S.A.)

[4] School of Chemistry, University of Leeds, Woodhouse Lane, Leeds, LS2 9JT (U.K.)

[5] Kavli Institute at Cornell for Nanoscale Science, Cornell University, Ithaca, New York 14853 (U.S.A.)

*co-corresponding authors, E-mail: lae37@cornell.edu; emily.asenath-smith@usace.army.mil

a) current address: U.S. Army Engineer Research and Development Center (ERDC), Cold Regions Research and Engineering Laboratory (CRREL), Hanover, NH 03755

Abstract: Building on the application of cuprite (Cu_2O) in solar energy technologies and reports of increased optical absorption caused by metal-to-semiconductor energy transfer, a confinement-based strategy was developed to fabricate high aspect ratio, crystalline Cu_2O nanorods containing entrapped gold nanoparticles (Au nps). Cu_2O was crystallized within the confines of track-etch membrane pores, where this physical, assembly-based method eliminates the necessity of specific chemical interactions to achieve a well-defined metal-semiconductor interface. With high-resolution scanning/transmission electron microscopy (S/TEM) and tomography, we demonstrate the encasement of the majority of Au nps by crystalline Cu_2O and show that crystalline Au-Cu_2O interfaces that are free of extended amorphous regions. Such nanocrystal heterostructures are good candidates for studying the transport physics of metal/semiconductor hybrids for optoelectronic applications.

Introduction

Cuprous oxide (Cu_2O) is a promising material in next-generation photovoltaic devices due to its favorable optoelectronic properties, earth-abundance, and low cost.[1-3] Integrating plasmonic assemblies into semiconducting materials can increase charge injection, optical path length, and enhance absorption of near IR light.[4-11] A key challenge that dictates the performance of such metal-semiconductor hybrid materials is achieving a metal-oxide interface that is free of electrically insulating organic ligands.[12-16] Methods to synthesize these materials generally require careful chemical design on a case-by-case basis.[7-9, 17] By introducing a physical control parameter (e.g., confinement within pores of track-etched membranes) to the crystallization microenvironment we designed a reaction system to achieve the encapsulation of Au nanoparticles within Cu_2O nanorods, regulating the assembly of a semiconductor-metal heterostructure without the introduction of organic structure-directing agents.

Originally explored as a synthesis template for electrochemical growth of nanotubes or nanorods of conducting polymers and metals,[18, 19] track-etched membranes have been used for the crystallization of transition metal oxides[20] and as synthetic models for studying crystallization in confinement.[21-29] Key outcomes of these works have included the ability to form high aspect ratio nanorods,[23, 26] and a route to interface semiconducting transition metal oxide nanowire arrays into macroscale structures with spatial control.[20] Up to this point, reports on electrochemical and solution-based crystallization within the pores of track-etched membranes have involved the formation of single phase or multilayered nanowires.[30-33] However, these membranes also present a means to physically control the encapsulation of (metal) nanoparticles within the target (semiconducting) crystalline nanorods, forming a crystal-within-a-crystal dual- (or multi-) phase material.

Within the (aqueous) crystallization microenvironment, the interaction between a host crystal and a guest material can be tuned by carefully controlling the crystallization kinetics (e.g., regulating the diffusion of reagents) and/or restricting the mobility of the guest materials.[34] This approach has been widely demonstrated for single crystal carbonates, where the encapsulation of organic colloids,[35] micelles,[36, 37] and fibers[38] has been achieved by the vapor diffusion of ammonium carbonate into an aqueous matrix (e.g., dispersion of particles or hydrogel) containing dissolved alkali metal salts.[39, 40] As an extension of this approach, we hypothesized that a solution-vapor phase crystallization of an oxide (e.g., Cu_2O) could be accomplished by the diffusion of a low vapor pressure basic species or reducing agent[41] into a transition metal oxide salt solution with the application of heat to drive the system to the oxide phase.[42]

Experimental Design. This article describes a new approach to synthesize metal-semiconductor hybrid materials. We crystallized cuprous oxide (Cu_2O) from aqueous solution at near ambient temperatures with hydrazine vapor diffusion as the reducing agent to regulate the crystallization kinetics. Growth within the confinement of track-etched membrane pores leads to the formation of high aspect ratio single crystal Cu_2O nanorods. We used this approach to entrap Au nps within the Cu_2O nanorods, without the need for large organic ligands on the nps. The structure of these hybrid materials was determined using high resolution scanning/transmission electron microscopy and tomography to demonstrate the encapsulation of numerous Au nps by crystalline Cu_2O and the crystalline nature of the Au-Cu_2O interface.

Results

Synthesis of Cu_2O Nanorods. Polycarbonate track-etched membranes (Fig. 1a) were used as crystallization templates for the formation of high aspect ratio Cu_2O nanorods. Using a modified Fehling's reaction, we induced the crystallization of Cu_2O from a (bright blue) basic solution of copper citrate using the vapor diffusion of hydrazine as a reducing agent.[43] Fehling's reaction

uses the formation of a red precipitate (Cu_2O) under heating of a basic copper citrate solution to indicate the presence of a reducing sugar (e.g., glucose).[44] By complexing the copper (II) ions with citrate, the precipitation of copper (II) hydroxide species is suppressed. Mechanistically, a basic species (OH^-) initiates the oxidation of the open chain aldehyde ($R - C^IOH$), forming a carboxylic acid ($R - C^{III}OOH$) and liberating two free electrons ($2e^-$) (Eq.1).

$$R - C^IOH + 2OH^- \rightarrow R - C^{III}OOH + H_2O + 2e^- \quad \text{Eq. 1}$$

The free electrons can then reduce chelated copper ions from oxidation state II to I (Eq. 2).

$$2Cu^{2+} + 2e^- \rightarrow 2Cu^+ \quad \text{Eq. 2}$$

Subsequent interaction of the cuprous (Cu^{2+}) ions with basic species leads to the crystallization of the mineral cuprite, Cu_2O (Eq. 3).

$$2Cu^+ + 2OH^- \rightarrow Cu_2O + H_2O \quad \text{Eq. 3}$$

The overall reaction is shown in Eq. 4.

$$R - C^IOH + 2Cu^{2+} + 4OH^- \rightarrow R - C^{III}OOH + Cu_2O + 2H_2O \quad \text{Eq. 4}$$

For the present study, the key point of Fehling's reagent is that crystallization of Cu_2O can be induced by the introduction of a (vapor phase) reducing agent to a basic solution containing a copper citrate complex.

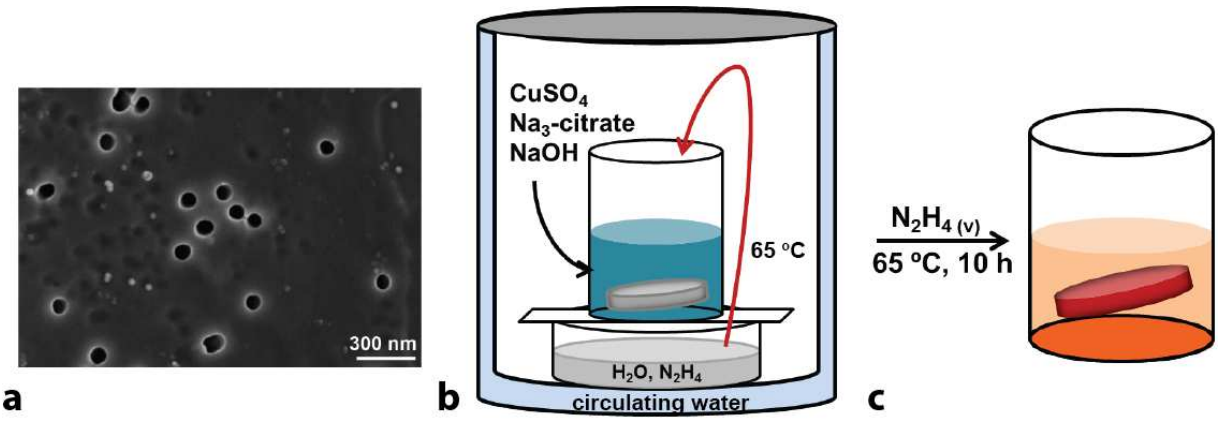

Figure 1. a) An SEM image of the surface of a track-etched membrane showing the uniformity of the cylindrical channels. b) Schematic representation of the double-walled crystallization chamber used for the growth of Cu_2O within the pores of track-etched membranes. The internal temperature of 65 ºC was accomplished by water circulation through the walls. The membranes were immersed in vials containing a basic, copper citrate solution that was set atop a petri dish containing a dilute solution of hydrazine hydrate. After sealing within the heated chamber, crystallization was induced by the vapor diffusion of hydrazine into the copper solution (denoted by curved red arrow). c) A graphical illustration of the post-crystallization state of the reaction solution and membrane. The reddish color is consistent with the formation of Cu_2O. The Cu_2O nanorods were isolated by dissolving the membranes in dichloromethane.

This reaction was carried out using a double-walled reaction chamber, and moderate heating (65 ºC) was achieved with circulating water (Fig. 1b). After reaction, the solution was a pale yellow and the membrane was a rusty red (Fig. 1c). The resulting crystalline nanorods (Fig. 2a) were extracted from the membrane channels by dissolving the membrane in dichloromethane. Individual rods exhibited selected area electron diffraction (SAED) patterns (Fig. 2b) that indexed to the cuprite (Cu_2O) phase of copper oxide.

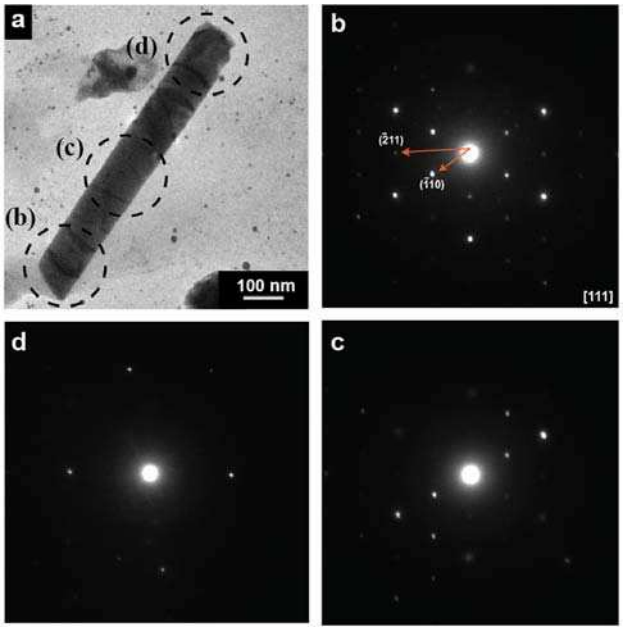

Figure 2. Crystallographic rotation occurs along the length of the Cu_2O nanorods grown within the track-etched membrane pores. (a) Bright field TEM of a crystalline Cu_2O nanorod showing dislocation lines (darker perpendicular lines) and highlighting the regions from which SAED patterns were taken. (b) The nanorod is positioned perpendicular to the [111] zone at the left most end, and is seen to rotate off axis along the length of the rod (c) and (d).

Uniformly straight nanorods (length=935±475 nm, width=112±13 nm, N=42, Fig. S1a,b) were seen under bright field TEM (Fig. 2a). Curved lines were seen to bisect the rods many times along their lengths; these features are consistent with the existence of dislocations, which are associated with both nanowire structures[44] and growth in confinement.[23] By taking SAED patterns at various positions along the length of the rods, we were able to observe a rotation of the cuprite lattice (Fig. 2b-d). No preferential crystallographic orientation of the rods with respect to their long axis was observed, where this observation is consistent with results from similar studies on calcite rods crystallized within the confines of track-etched membranes.[45] In contrast with other Cu_2O synthesis approaches which involve electrodeposition[46] or high-temperature vapor deposition,[47] the nanorods reported here can be crystallized from aqueous solutions at near ambient temperatures without an applied potential. In addition, the track-

etched membranes can be used as a vehicle to transfer spatially organized arrays of nanorods to various macroscale substrates.[20]

Synthesis of Cu_2O-Au Heterostructures. To achieve the formation of Cu_2O-Au nanocrystal heterostructures within the confines of polycarbonate track-etched membranes pores, we first immobilized Au nanoparticles (d=16±1 nm, Fig. S2) in the membrane channels via vacuum filtration of citrate-stabilized Au nanoparticle solutions (dialyzed to pH 10, NaOH) (Fig. 3a). With disordered arrays of gold nanoparticles entrapped within the membrane pores prior to crystallization, Cu_2O encapsulated the Au nanoparticles during growth, forming high aspect ratio, metal-semiconductor heterostructures (length=997±393 nm, width=106±11 nm, N=52, Fig. S1c,d). After crystallization, the Cu_2O-Au nanorods were isolated by washing with dichloromethane to remove the membrane (Fig. S3). Formation of the Cu_2O crystalline phase was confirmed by SAED (Fig. S4), and by electron energy loss spectroscopy (EELS, Fig. 4a-c), which showed the characteristic signature of Cu(I) oxidation state.[48, 49]

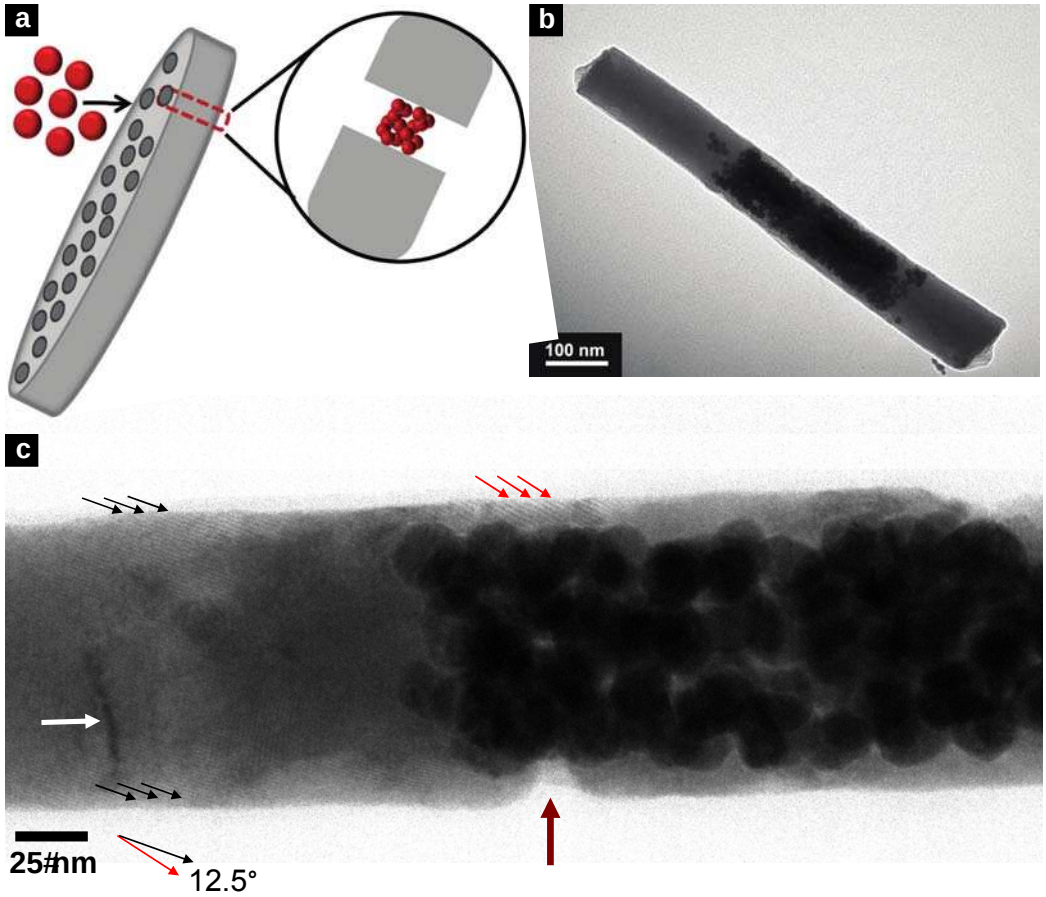

Figure 3. (a) Cartoon of the method used to assemble Au np arrays within the pores (d = 0.05 μm) of track-etched membranes prior to crystallization. The citrate-stabilized Au nps (11 ± 1 nm) were immobilized within the confines the cylindrical membrane channels by vacuum filtration. Subsequent crystallization (as described in text and Fig. 1) resulted in the encapsulation of the Au np array within the crystalline Cu_2O nanorods. (b) Bright field TEM image of a single Cu_2O-Au nanorod formed by growth within the channels of track etched membrane pores that were preloaded with Au np. The darker central region is the encapsulated Au np array. (c) A higher magnification of a Cu_2O-Au nanorod highlighting the defect features: i) Dislocations appear as the dark curved line at left of rod (white arrow); ii) Continuous Moiré fringes from the crystal were observed across the width of the Cu_2O nanorod and extending down the length of much of the rod. The directions of the fringes are marked with arrows. A progressive rotation in the fringe angle can be seen along the length of the rod, amounting to a rotation of ~12.5° over roughly 200 nm. A surface discontinuity (notch) in the rod is highlighted with a vertical (red) arrow. (Note: the nanorod shown in panel c is different than the one featured in panel b.)

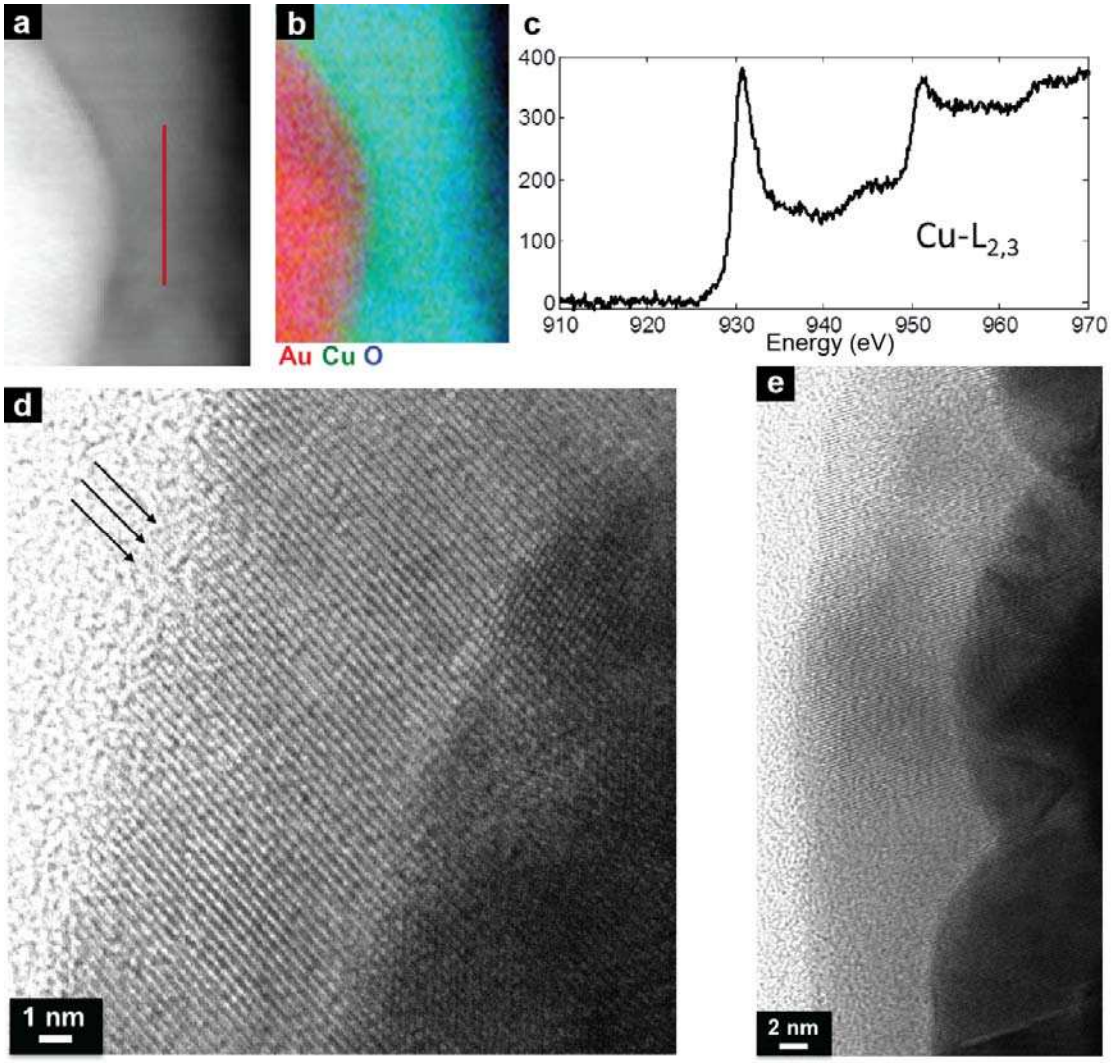

Figure 4. (a) Bright-field STEM image of the analysis region selected from a Cu_2O-Au nanorod. (b) Elemental map derived from electron energy loss spectra (EELS) chemically verifying that a copper oxide surrounds the Au nanoparticle. (c) EELS fine structure, acquired along the red line denoted in panel (a), confirming the Cu(I) oxidation state. (d) High-resolution BF-STEM of the Cu_2O-Au interface, illustrating lattice fringes (highlighted with arrows) of the crystalline Cu_2O nanorod surrounding the edge of crystalline Au nanoparticle. The Au and Cu_2O interface appears without any extended amorphous region or phase change of materials. (e) Overview of multiple Au np within the crystalline Cu_2O rod, showing continuous Cu_2O lattice fringes across multiple Au nps.

Under bright field (BF) S/TEM, the Au nanoparticle array appeared to be completely encapsulated within the high aspect ratio crystalline Cu_2O rod (Fig. 3b,c). In common with the

single-phase Cu_2O nanorods, dislocations are visible in the Cu_2O-Au nanocrystal heterostructures (Fig. 3c). Likewise, the lattice rotations seen in the single-phase Cu_2O nanorods (Fig. 2) are also observed in the SAED patterns of the nanocomposite Cu_2O-Au architectures; the SAED patterns (Fig. S4) show off axis tilting and high magnification TEM imaging reveals Moiré fringes that rotate ~12.5º over 200 nm (Fig. 3c). In addition to the linear defects, surface discontinuities were seen in the Cu_2O-Au crystals (notch in Fig. 3c). Further examination of the single-phase Cu_2O and the Cu_2O-Au nanorods (Fig. S5) revealed that both contain dislocations and surface discontinuities. These defects are not specifically caused by the presence of the Au nanoparticle array, but rather seem to be a signature of the high aspect ratio structure and/or growth conditions.[44, 45, 50, 51]

High-resolution Characterization of Cu_2O-Au Heterostructures. The uniqueness of our Cu_2O-Au heterostructures in the field of metal-semiconductor hybrid nanostructures,[10] and the potential generalizability of this synthesis approach to a range of crystalline materials, prompted us to interrogate structural characteristics of the interface between the Cu_2O host crystal and the encapsulated Au nanocrystals. As both Cu_2O and Au are stable under electron beam exposure, we were able to perform detailed structural analyses to determine whether the Cu_2O crystal was continuous throughout the Au nanoparticle array and to characterize the Cu_2O-Au interface to look for amorphous regions or extended defects, which may affect electrical transport between the two materials.

STEM tomography was performed on an individual Cu_2O-Au nanorod to probe the entire 3D structure (Movie S1). Single projection images (Fig. 5a) and slices through the 3D tomographic reconstruction (Fig. 5b,d) confirm the encapsulation of the Au nps within the Cu_2O nanorods. The contrast difference between the two materials was used to generate an isosurface rendering of both the Au nps (green) and the Cu_2O matrix (purple) (Fig. 5c). By combining

individual tomographic slices with the corresponding slices through the isosurface rendering, the continuity of the Cu_2O crystal through the encapsulated Au np array was studied. Visible as a pale blue matrix surrounding the orange particles (Fig. 5d), Cu_2O encapsulates the Au nps without obvious discontinuities within the nanoparticle array. Three dimensional imaging also reveals notches and voids within the Cu_2O nanorod, though not associated with the Au nps. In particular, discontinuous voids within the nanorod center are clearly visualized in the tomographic slices (Fig. 5b).

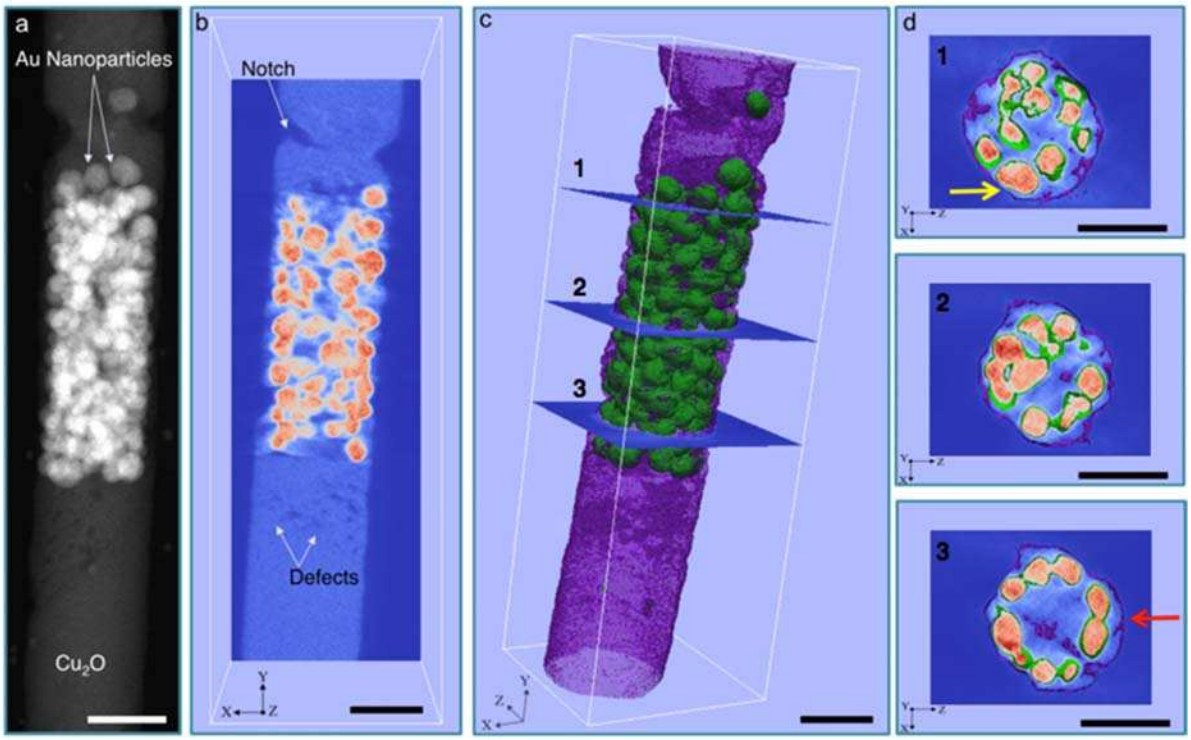

Figure 5. Tomographic reconstruction of the 3D structure of a Cu_2O-Au nanorod taken with STEM: (a) Single projection slice from the original tilt series. (b) The tomographic orthoslice confirms the encapsulation of the Au np (orange) within the Cu_2O nanorods (pale blue). Defects are indicated by arrows in the image. (c) The isosurface rendering of the structure shows the encapsulation of the Au np (green) by the Cu_2O nanorod (purple). Opacity of the nanorod isosurface in (c) is reduced to reveal interior nanoparticles. (d) Subtomograms (Z = 6 slices, ~3 nm) of the nanocomposite system and their corresponding isosurfaces (Au np = green isosurface; Cu_2O nanorod = purple isosurface) as indicated in (c), showing encapsulation of the Au np array within the Cu_2O crystal. Some nanoparticles, such as those demarcated by the yellow arrow, are shallowly encapsulated. Most nanoparticles are well included by the Cu_2O crystal, such as those indicated by the red arrow. *Scale bars = 50 nm*.

To further understand the interface between the Cu_2O crystal and the encapsulated Au nps, we also performed high-resolution STEM imaging (Fig. 4d,e). Looking closely at the interface between a single Au nanoparticle and the encapsulating Cu_2O crystal (Fig. 4d) we see that fringes from each lattice meet directly at the boundary between the two crystals. While here the images were obtained in projection through the nanorod and the atomic lattice from the Cu_2O above and below the Au nps have to be taken into account, there is no evidence for extensive amorphous regions or planar lattice defects at the Cu_2O-Au interface. In addition, we find continuous Cu_2O lattice fringes that extend over numerous particles (Fig. 4e). This continuity suggests the complete encapsulation of multiple Au nps within a single crystalline Cu_2O domain.

Discussion

Encapsulation of Particles in Single Crystals. The confinement-based approach introduced here provides a novel route to creating hybrid nanostructures with control over the interface between the host crystal and encapsulated nanoparticles. The entrapment of guest materials, which are larger than small molecules, within a host crystal is well-recognized in certain geologic minerals, such as "rutile-in-quartz",[52, 53] and also in biominerals.[34, 54, 55] The successful entrapment of polymeric guests within single crystals, primarily of calcite, has been widely demonstrated,[34, 35, 55, 56] relying either on the chemical functionality of the polymers, or in some cases, on the restricted mobility of the guest species.[34, 35, 57] The encapsulation of inorganic and metallic guest particles has only been achieved by functionalizing the nanoparticles with diblock copolymers,[58, 59] or immobilizing them within hydrogel matrices.[39, 40] In all of these cases, the encapsulated nanoparticles are surrounded by an insulating organic layer at the interface between the guest nanoparticle and the host crystalline material. In electronic materials, such an insulating layer would be a barrier to the transport of carriers between the two crystalline materials.

In contrast to carbonate materials, very few oxide compounds have been demonstrated to encapsulate guest particles while remaining as single crystals.[60-62] Most work has focused on the occlusion of polymeric colloids (100's of nm) within zinc and copper oxides, where occlusion was achieved by tuning the surface chemistry of the particles. Carboxylate functionality has been associated with the successful encapsulation of polystyrene spheres,[56, 63] while amine surface moieties have directed the interaction of copper oxide with surfaces.[43, 64] Such findings complicate the development of new multi-functional materials as it is challenging to predict which chemical functionality is needed on a (nanoparticle) surface to favor its encapsulation/interaction with/in a single crystal host.

As an alternative to surface functionalization, colloidal crystal templates have been used to physically entrap guest particles within host crystals. Electrochemical methods have been used to grow Cu_2O around a template of polystyrene spheres, embedding the colloids within the single crystal host.[65, 66] In addition, the confinement provided by a wedge was used to precipitate calcite single crystals within colloidal crystals of polystyrene spheres.[35] The method described here is an extension of this approach, where we have demonstrated that by performing crystallization within a confined volume, the interaction of two dissimilar crystals can be controlled without high demands on the surface chemistry. In addition, our current work with track-etched membranes has allowed us to regulate the interaction between two crystalline materials at much smaller length scales than previously reported.

Characterization of the Host-Guest Interface. Our metal oxide/metal nanoparticle system also provided us with an opportunity to characterize the interface between the two phases. While polymeric spheres have been incorporated into inorganic crystals, attempts to study the interfaces have been limited by the amorphous structure of the polymer spheres and the low atomic numbers of their constituents. Further, although a range of calcite/inorganic nanoparticle

single crystal nanocomposites have been synthesized, the interface between the two materials cannot be readily studied using TEM-based techniques due to the beam-sensitivity of $CaCO_3$. As a consequence, we still have a relatively poor understanding of the structural relationships between the guest particles and the host crystal phases, and the structure of the interface between these components.

The nanocrystal heterostructures synthesized here were both stable to the electronic beam and of nanoscale dimensions. Their structure can therefore be directly studied using high resolution electron microscopy without the introduction of preparation artifacts. Our results show that there is a high degree of crystallographic order at the boundary between the two different crystalline materials (Fig. 4d,e), but no epitaxial relationship between the Au and Cu_2O lattices. This interface structure, and the continuous intergrowth of Cu_2O throughout the Au np array (Fig. 5), suggest that the growth of the cuprite rods is independent of the Au nps, and does not originate from them. This growth mechanism is in contrast to reports of nanorods grown epitaxially from single nanoparticles or nanoparticles that are epitaxially nucleated on the surfaces of nanorods.[67-70] Recent in situ AFM studies of the entrapment of polymeric micelles within calcite crystals has shown that the micelles bind preferentially to the step edges, which then experience little or no inhibition as the calcite lattice grows around the adsorbed micelles.[71] Further, the relatively compliant micelles experience lateral compression as they are occluded in the crystal, where this distortion gives rise to a cavity within the calcite. Although elegant, these AFM studies could not demonstrate whether the observed cavities are ultimately retained or lost, after nanoparticle occlusion. The continuous interface observed between the Au np and Cu_2O observed here suggests that with stiff “guests” no such cavity forms and the crystal grows around the obstacle, creating “tight fit” (Fig. 4). Finally, the observation of multiple Au nps within a single Cu_2O coherent domain (Fig. 4e) indicates that the cuprite crystal is able to grow around

the particles without significant disruption to its lattice, in agreement with similar reports for particle and fiber encapsulation within calcite.[36, 38]

Optoelectronic Properties of Metal-Semiconductor Heterostructures. The metal-semiconductor heterostructures synthesized in this work represent an example of a new geometrical configuration: an array of plasmonic nanoparticles encased within a crystalline semiconductor, with interfaces free of insulating organic material. Interest in these types of heterostructures primarily relates to changes in the localized surface plasmon resonance (LSPR) of the metal nanoparticles in the presence of the semiconductor and changes in electron transfer from the metal into the semiconductor.[10] Based on the plasmon hybridization model for assemblies of nps, we expect the plasmonic properties to be retained in our Au-Cu_2O heterostructures, and to potentially become more complex, resulting in splitting of the single plasmon peak into low and high energy coupled (hybridized) modes.[72, 73] As compared to discrete core-shell architectures, the Au nps in our rods have varying lengths of contact between them. For example, some nps appear to exist as isolated individuals (Fig. 5d1), while others are present as dimers (Fig. 5d3), or have contacts with multiple Au nps (Fig. 5d2). These features could give rise to diverse splitting, and thus broadening, of the plasmon peak in these materials. Chains of plasmonic particles have also been associated with the emergence of Fano resonance, and the electric field enhancements are observed in both linear and kinked chains.[5]

Conclusions

In this work, we have demonstrated that crystallization in confinement provides a promising route for generating nanocrystal heterostructures comprising Au nps embedded within a crystalline Cu_2O host. Importantly, this strategy leads to a clean interface between the host crystal and occluded nanoparticles. We report high-resolution, 3-D structural characterization that shows that the Cu_2O crystal is continuous throughout the Au nanoparticle array and that the

interface between the two crystals is highly ordered. Our approach is envisaged to be quite general, where the ability to make metal-semiconductor hybrid nanostructures, or even heterostructures from two different semiconductors, without complex chemical considerations, presents new opportunities to the field of advanced materials. Hybrid crystalline materials, which are predicted to have emergent properties, can now be accessed and studied for a wide range of optoelectronic applications.

ACKNOWLEDGMENTS

We acknowledge support from the NSF (DMR 1210304) and EAS acknowledges the NSF Graduate Research Fellowship (GRF, DGE-0707428), and Integrative Graduate Education and Research Traineeship (IGERT, DGE-0903653) Programs. This work was also supported in part by the Cornell Center for Materials Research (CCMR) and made use of the CCMR Shared Facilities, both funded by NSF MRSEC program (DMR 1120296). We also acknowledge support from an Engineering and Physical Sciences Research Council (EPSRC) Materials World Network grant (EP/J018589/1, FCM) and EPSRC grant EP/K006304/1 (FCM and ANK). Specific acknowledgment is made for the assistance of Malcolm G. Thomas and John L. Grazul during the use of the electron microscopy facilities.

Supporting Information

Materials and methods, Figures S1-S5, and Movie S1: supplemental TEM and SAED images and tomographic reconstruction are included in supporting information. This material is available free of charge via the internet at http://pubs.acs.org.

REFERENCES:

1. Wong, T. K. S.; Zhuk, S.; Masudy-Panah, S.; Dalapati, G. K., Current Status and Future Prospects of Copper Oxide Heterojunction Solar Cells. *Materials* **2016,** *9*, 271.
2. Shang, Y.; Guo, L., Facet-Controlled Synthetic Strategy of Cu_2O-Based Crystals for Catalysis and Sensing. *Adv. Sci.* **2015,** *2*, 1500140.
3. Meyer, B. K.; Polity, A.; Reppin, D.; Becker, M.; Hering, P.; Klar, P. J.; Sander, T.; Reindl, C.; Benz, J.; Eickhoff, M.; Heiliger, C.; Heinemann, M.; Blaesing, J.; Krost, A.; Shokovets, S.; Mueller, C.; Ronning, C., Binary copper oxide semiconductors: From materials towards devices. *Phys. Status Solidi B* **2012,** *249*, 1487-1509.
4. Atwater, H. A.; Polman, A., Plasmonics for improved photovoltaic devices. *Nature Mater.* **2010,** *9*, 205-213.
5. Klinkova, A.; Choueiri, R. M.; Kumacheva, E., Self-assembled plasmonic nanostructures. *Chem. Soc. Rev.* **2014,** *43*, 3976-3991.
6. Cushing, S. K.; Li, J. T.; Meng, F. K.; Senty, T. R.; Suri, S.; Zhi, M. J.; Li, M.; Bristow, A. D.; Wu, N. Q., Photocatalytic Activity Enhanced by Plasmonic Resonant Energy Transfer from Metal to Semiconductor. *J. Am. Chem. Soc.* **2012,** *134*, 15033-15041.
7. Wang, X.; Peng, K. Q.; Hu, Y.; Zhang, F. Q.; Hu, B.; Li, L.; Wang, M.; Meng, X. M.; Lee, S. T., Silicon/Hematite Core/Shell Nanowire Array Decorated with Gold Nanoparticles for Unbiased Solar Water Oxidation. *Nano Lett.* **2014,** *14*, 18-23.
8. Zhang, L.; Blom, D. A.; Wang, H., Au-Cu_2O Core-Shell Nanoparticles: A Hybrid Metal-Semiconductor Heteronanostructure with Geometrically Tunable Optical Properties. *Chem. Mater.* **2011,** *23*, 4587-4598.
9. Pan, Y. L.; Deng, S. Z.; Polavarapu, L.; Gao, N. Y.; Yuan, P. Y.; Sow, C. H.; Xu, Q. H., Plasmon-Enhanced Photocatalytic Properties of Cu_2O Nanowire-Au Nanoparticle Assemblies. *Langmuir* **2012,** *28*, 12304-12310.
10. Jiang, R.; Li, B.; Fang, C.; Wang, J., Metal/Semiconductor Hybrid Nanostructures for Plasmon-Enhanced Applications. *Adv. Mater.* **2014,** *26*, 5274-5309.
11. Nepal, D.; Drummy, L. F.; Biswas, S.; Park, K.; Vaia, R. A., Large Scale Solution Assembly of Quantum Dot–Gold Nanorod Architectures with Plasmon Enhanced Fluorescence. *ACS Nano* **2013,** *7*, 9064-9074.
12. Baumgardner, W. J.; Whitham, K.; Hanrath, T., Confined-but-Connected Quantum Solids via Controlled Ligand Displacement. *Nano Lett.* **2013,** *13*, 3225-3231.
13. Kovalenko, M. V.; Scheele, M.; Talapin, D. V., Colloidal Nanocrystals with Molecular Metal Chalcogenide Surface Ligands. *Science* **2009,** *324*, 1417-1420.
14. Evers, W. H.; Goris, B.; Bals, S.; Casavola, M.; de Graaf, J.; Roij, R. v.; Dijkstra, M.; Vanmaekelbergh, D., Low-Dimensional Semiconductor Superlattices Formed by Geometric Control over Nanocrystal Attachment. *Nano Lett.* **2013,** *13*, 2317-2323.
15. Boneschanscher, M. P.; Evers, W. H.; Geuchies, J. J.; Altantzis, T.; Goris, B.; Rabouw, F. T.; van Rossum, S. A. P.; van der Zant, H. S. J.; Siebbeles, L. D. A.; Van Tendeloo, G.; Swart, I.; Hilhorst, J.; Petukhov, A. V.; Bals, S.; Vanmaekelbergh, D., Long-range orientation and atomic attachment of nanocrystals in 2D honeycomb superlattices. *Science* **2014,** *344*, 1377-1380.
16. Wei, J.; Jiang, N.; Xu, J.; Bai, X.; Liu, J., Strong Coupling between ZnO Excitons and Localized Surface Plasmons of Silver Nanoparticles Studied by STEM-EELS. *Nano Lett.* **2015,** *15*, 5926-5931.
17. Kuo, C. H.; Yang, Y. C.; Gwo, S.; Huang, M. H., Facet-Dependent and Au Nanocrystal-Enhanced Electrical and Photocatalytic Properties of Au-Cu_2O Core-Shell Heterostructures. *J. Am. Chem. Soc.* **2011,** *133*, 1052-1057.
18. Martin, C. R., Membrane-based synthesis of nanomaterials. *Chem. Mater.* **1996,** *8*, 1739-1746.

19. Martin, C. R., Nanomaterials - A Membrane-Based Synthetic Approach. *Science* **1994,** *266*, 1961-1966.
20. Zhou, H. J.; Wong, S. S., A facile and mild synthesis of 1-D ZnO, CuO, and alpha-Fe_2O_3 nanostructures and nanostructured arrays. *ACS Nano* **2008,** *2*, 944-958.
21. Whittaker, M. L.; Dove, P. M.; Joester, D., Nucleation on surfaces and in confinement. *MRS Bull.* **2016,** *41*, 388-392.
22. Jiang, Q.; Ward, M. D., Crystallization under nanoscale confinement. *Chem. Soc. Rev.* **2014,** *43*, 2066-2079.
23. Kim, Y. Y.; Hetherington, N. B. J.; Noel, E. H.; Kroger, R.; Charnock, J. M.; Christenson, H. K.; Meldrum, F. C., Capillarity Creates Single-Crystal Calcite Nanowires from Amorphous Calcium Carbonate. *Angew. Chem. Int. Ed.* **2011,** *50*, 12572-12577.
24. Loste, E.; Park, R. J.; Warren, J.; Meldrum, F. C., Precipitation of calcium carbonate in confinement. *Adv. Funct. Mater.* **2004,** *14*, 1211-1220.
25. Loste, E.; Meldrum, F. C., Control of calcium carbonate morphology by transformation of an amorphous precursor in a constrained volume. *Chem. Commun.* **2001**, 901-902.
26. Schenk, A. S.; Albarracin, E. J.; Kim, Y. Y.; Ihli, J.; Meldrum, F. C., Confinement stabilises single crystal vaterite rods. *Chem. Commun.* **2014,** *50*, 4729-4732.
27. Stephens, C. J.; Ladden, S. F.; Meldrum, F. C.; Christenson, H. K., Amorphous Calcium Carbonate is Stabilized in Confinement. *Adv. Funct. Mater.* **2010,** *20*, 2108-2115.
28. Cantaert, B.; Beniash, E.; Meldrum, F. C., Nanoscale Confinement Controls the Crystallization of Calcium Phosphate: Relevance to Bone Formation. *Chem. Eur. J.* **2013,** *19*, 14918-14924.
29. Cantaert, B.; Beniash, E.; Meldrum, F. C., The role of poly(aspartic acid) in the precipitation of calcium phosphate in confinement. *J. Mater. Chem. B* **2013,** *1*, 6586-6595.
30. Whitney, T. M.; Jiang, J. S.; Searson, P. C.; Chien, C. L., Fabrication and Magnetic-Properties of Arrays of Metallic Nanowires. *Science* **1993,** *261*, 1316-1319.
31. Salem, A. K.; Chen, M.; Hayden, J.; Leong, K. W.; Searson, P. C., Directed assembly of multisegment Au/Pt/Au nanowires. *Nano Lett.* **2004,** *4*, 1163-1165.
32. Martin, B. R.; Dermody, D. J.; Reiss, B. D.; Fang, M. M.; Lyon, L. A.; Natan, M. J.; Mallouk, T. E., Orthogonal self-assembly on colloidal gold-platinum nanorods. *Adv. Mater.* **1999,** *11*, 1021-1025.
33. Chen, M.; Chien, C. L.; Searson, P. C., Potential modulated multilayer deposition of multisegment Cu/Ni nanowires with tunable magnetic properties. *Chem. Mater.* **2006,** *18*, 1595-1601.
34. Asenath-Smith, E.; Li, H. Y.; Keene, E. C.; Seh, Z. W.; Estroff, L. A., Crystal Growth of Calcium Carbonate in Hydrogels as a Model of Biomineralization. *Adv. Funct. Mater.* **2012,** *22*, 2891-2914.
35. Hetherington, N. B. J.; Kulak, A. N.; Kim, Y. Y.; Noel, E. H.; Snoswell, D.; Butler, M.; Meldrum, F. C., Porous Single Crystals of Calcite from Colloidal Crystal Templates: ACC is Not Required for Nanoscale Templating. *Adv. Funct. Mater.* **2011,** *21*, 948-954.
36. Kim, Y. Y.; Ganesan, K.; Yang, P. C.; Kulak, A. N.; Borukhin, S.; Pechook, S.; Ribeiro, L.; Kroger, R.; Eichhorn, S. J.; Armes, S. P.; Pokroy, B.; Meldrum, F. C., An artificial biomineral formed by incorporation of copolymer micelles in calcite crystals. *Nature Mater.* **2011,** *10*, 890-896.
37. Kim, Y.-Y.; Semsarilar, M.; Carloni, J. D.; Cho, K. R.; Kulak, A. N.; Polishchuk, I.; Hendley, C. T.; Smeets, P. J. M.; Fielding, L. A.; Pokroy, B.; Tang, C. C.; Estroff, L. A.; Baker, S. P.; Armes, S. P.; Meldrum, F. C., Structure and Properties of Nanocomposites Formed by the Occlusion of Block Copolymer Worms and Vesicles Within Calcite Crystals. *Adv. Funct. Mater.* **2016,** *26*, 1382-1392.
38. Li, H. Y.; Xin, H. L.; Muller, D. A.; Estroff, L. A., Visualizing the 3D Internal Structure of Calcite Single Crystals Grown in Agarose Hydrogels. *Science* **2009,** *326*, 1244-1247.
39. Liu, Y.; Yuan, W.; Shi, Y.; Chen, X.; Wang, Y.; Chen, H.; Li, H., Functionalizing Single Crystals: Incorporation of Nanoparticles Inside Gel-Grown Calcite Crystals. *Angew. Chem. Int. Ed.* **2014,** *53*, 4127-4131.
40. Kim, Y.-Y.; Schenk, A. S.; Walsh, D.; Kulak, A. N.; Cespedes, O.; Meldrum, F. C., Bio-inspired formation of functional calcite/metal oxide nanoparticle composites. *Nanoscale* **2014,** *6*, 852-859.

41. Ding, Y.; Chen, M. W.; Erlebacher, J., Metallic mesoporous nanocomposites for electrocatalysis. *J. Am. Chem. Soc.* **2004,** *126*, 6876-6877.
42. Matijevic, E., Preparation and Properties of Uniform Size Colloids. *Chem. Mater.* **1993,** *5*, 412-426.
43. DiCorato, A. E.; Asenath-Smith, E.; Kulak, A. N.; Meldrum, F. C.; Estroff, L. A., Cooperative Effects of Confinement and Surface Functionalization Enable the Formation of Au/Cu2O Metal–Semiconductor Heterostructures. *Cryst. Growth Des.* **2016**, 10.1021/acs.cgd.6b00913.
44. Hacialioglu, S.; Meng, F.; Jin, S., Facile and mild solution synthesis of Cu_2O nanowires and nanotubes driven by screw dislocations. *Chem. Commun.* **2012,** *48*, 1174-1176.
45. Verch, A.; Cote, A. S.; Darkins, R.; Kim, Y. Y.; van de Locht, R.; Meldrum, F. C.; Duffy, D. M.; Kroger, R., Correlation between Anisotropy and Lattice Distortions in Single Crystal Calcite Nanowires Grown in Confinement. *Small* **2014,** *10*, 2697-2702.
46. Oku, T.; Yamada, T.; Fujimoto, K.; Akiyama, T., Microstructures and Photovoltaic Properties of Zn(Al)O/Cu_2O-Based Solar Cells Prepared by Spin-Coating and Electrodeposition. *Coatings* **2014,** *4*, 203-213.
47. Brittman, S.; Yoo, Y.; Dasgupta, N. P.; Kim, S. I.; Kim, B.; Yang, P. D., Epitaxially Aligned Cuprous Oxide Nanowires for All-Oxide, Single-Wire Solar Cells. *Nano Lett.* **2014,** *14*, 4665-4670.
48. Wu, L. H.; Yang, J.; Chi, M. F.; Wang, S. Y.; Wei, P.; Zhang, W. Q.; Chen, L. D.; Yang, J. H., Enhanced Thermoelectric Performance in Cu-Intercalated BiTeI by Compensation Weakening Induced Mobility Improvement. *Sci. Rep.* **2015,** *5*, 14319.
49. Leapman, R. D.; Grunes, L. A.; Fejes, P. L., Study of the L23 Edges in the 3D Transition-Metals and their Oxides by Electron-Energy-Loss Spectroscopy with Comparisons to Theory. *Phys. Rev. B* **1982,** *26*, 614-635.
50. Akatyeva, E.; Dumitrica, T., Eshelby Twist and Magic Helical Zinc Oxide Nanowires and Nanotubes. *Phys. Rev. Lett.* **2012,** *109*, 035501.
51. Meng, F.; Jin, S., The Solution Growth of Copper Nanowires and Nanotubes is Driven by Screw Dislocations. *Nano Lett.* **2012,** *12*, 234-239.
52. Moses, A. J.; Parsons, C. L., *Elements of Mineralogy, Crystallography and Blowpipe Analysis* D. Van Nostrand: New York, 1920.
53. Buckley, H., Examples of the 'Rutile in Quartz' Phenomenon in Artificial Crystals. *Z. Kristallogr.* **1934,** *88*, 181-184.
54. Li, H. Y.; Xin, H. L.; Kunitake, M. E.; Keene, E. C.; Muller, D. A.; Estroff, L. A., Calcite Prisms from Mollusk Shells (Atrina Rigida): Swiss-cheese-like Organic–Inorganic Single-crystal Composites. *Adv. Funct. Mater.* **2011,** *21*, 2028-2034.
55. Weber, E.; Pokroy, B., Intracrystalline inclusions within single crystalline hosts: from biomineralization to bio-inspired crystal growth. *CrystEngComm* **2015,** *17*, 5873-5883.
56. Lu, C. H.; Qi, L. M.; Cong, H. L.; Wang, X. Y.; Yang, J. H.; Yang, L. L.; Zhang, D. Y.; Ma, J. M.; Cao, W. X., Synthesis of calcite single crystals with porous surface by templating of polymer latex particles. *Chem. Mater.* **2005,** *17*, 5218-5224.
57. Li, H. Y.; Estroff, L. A., Calcite Growth in Hydrogels: Assessing the Mechanism of Polymer Network Incorporation into Single Crystals. *Adv. Mater.* **2009,** *21*, 470-473.
58. Kulak, A. N.; Semsarilar, M.; Kim, Y. Y.; Ihli, J.; Fielding, L. A.; Cespedes, O.; Armes, S. P.; Meldrum, F. C., One-pot synthesis of an inorganic heterostructure: uniform occlusion of magnetite nanoparticles within calcite single crystals. *Chem. Sci.* **2014,** *5*, 738-743.
59. Kulak, A. N.; Yang, P. C.; Kim, Y. Y.; Armes, S. P.; Meldrum, F. C., Colouring crystals with inorganic nanoparticles. *Chem. Commun.* **2014,** *50*, 67-69.
60. Thiry, D.; Molina-Luna, L.; Gautron, E.; Stephant, N.; Chauvin, A.; Du, K.; Ding, J.; Choi, C.-H.; Tessier, P.-Y.; El Mel, A.-A., The Kirkendall Effect in Binary Alloys: Trapping Gold in Copper Oxide Nanoshells. *Chem. Mater.* **2015,** *27*, 6374-6384.

61. Cargnello, M.; Johnston-Peck, A. C.; Diroll, B. T.; Wong, E.; Datta, B.; Damodhar, D.; Doan-Nguyen, V. V. T.; Herzing, A. A.; Kagan, C. R.; Murray, C. B., Substitutional doping in nanocrystal superlattices. *Nature* **2015,** *524*, 450-453.
62. Kulak, A. N.; Grimes, R.; Kim, Y.-Y.; Semsarilar, M.; Anduix-Canto, C.; Cespedes, O.; Armes, S. P.; Meldrum, F. C., Polymer-Directed Assembly of Single Crystal Zinc Oxide/ Magnetite Nanoparticle Nanocomposites under Standard and Hydrothermal Conditions. *Chem. Mater.* **2016**, acs.chemmater.6b03563.
63. Munoz-Espi, R.; Qi, Y.; Lieberwirth, I.; Gomez, C. M.; Wegner, G., Surface-functionalized latex particles as controlling agents for the mineralization of zinc oxide in aqueous medium. *Chem. Eur. J.* **2006,** *12*, 118-129.
64. Susman, M. D.; Feldman, Y.; Vaskevich, A.; Rubinstein, I., Chemical Deposition of Cu_2O Nanocrystals with Precise Morphology Control. *ACS Nano* **2014,** *8*, 162-174.
65. Li, X.; Jiang, Y.; Shi, Z.; Xu, Z., Two growth modes of metal oxide in the colloidal crystal template leading to the formation of two different macroporous materials. *Chem. Mater.* **2007,** *19*, 5424-5430.
66. Li, X.; Tao, F.; Jiang, Y.; Xu, Z., 3-D ordered macroporous cuprous oxide: Fabrication, optical, and photoelectrochemical properties. *J. Colloid Interface Sci.* **2007,** *308*, 460-465.
67. Costi, R.; Saunders, A. E.; Banin, U., Colloidal Hybrid Nanostructures: A New Type of Functional Materials. *Angew. Chem. Int. Ed.* **2010,** *49*, 4878-4897.
68. Fan, F.-R.; Ding, Y.; Liu, D.-Y.; Tian, Z.-Q.; Wang, Z. L., Facet-Selective Epitaxial Growth of Heterogeneous Nanostructures of Semiconductor and Metal: ZnO Nanorods on Ag Nanocrystals. *J. Am. Chem. Soc.* **2009,** *131*, 12036-12037.
69. Figuerola, A.; van Huis, M.; Zanella, M.; Genovese, A.; Marras, S.; Falqui, A.; Zandbergen, H. W.; Cingolani, R.; Manna, L., Epitaxial CdSe-Au Nanocrystal Heterostructures by Thermal Annealing. *Nano Lett.* **2010,** *10*, 3028-3036.
70. Habas, S. E.; Lee, H.; Radmilovic, V.; Somorjai, G. A.; Yang, P., Shaping binary metal nanocrystals through epitaxial seeded growth. *Nature Mater.* **2007,** *6*, 692-697.
71. Cho, K. R.; Kim, Y.-Y.; Yang, P.; Cai, W.; Pan, H.; Kulak, A. N.; Lau, J. L.; Kulshreshtha, P.; Armes, S. P.; Meldrum, F. C.; De Yoreo, J. J., Direct observation of mineral-organic composite formation reveals occlusion mechanism. *Nat. Commun.* **2016,** *7*, 10187.
72. Prodan, E.; Radloff, C.; Halas, N. J.; Nordlander, P., A Hybridization Model for the Plasmon Response of Complex Nanostructures. *Science* **2003,** *302*, 419-422.
73. Halas, N. J.; Lal, S.; Chang, W.-S.; Link, S.; Nordlander, P., Plasmons in Strongly Coupled Metallic Nanostructures. *Chem. Rev.* **2011,** *111*, 3913-3961.

For Table of Contents Use Only